Title

Acoustic Spark Chamber

Permalink

https://escholarship.org/uc/item/4xc248hj

Authors

Maglić, Bogdan C
Kirsten, Frederick A

Publication Date

1962-05-01

University of California

Ernest O. Lawrence Radiation Laboratory

DISCLAIMER

cy 2

UNIVERSITY OF CALIFORNIA

Lawrence Radiation Laboratory
Berkeley, California

Contract No. W-7405-eng-48

ERRATA

June 14, 1962

TO: All recipients of UCRL-10057

FROM: Technical Information Division

SUBJECT: UCRL-10057, "Acoustic Spark Chamber" by Bogdan C. Maglić and Frederick A. Kirsten, dated May 2, 1962.

Page	Line	From	Reads	Should Read
iii	2	bottom	... three probes per gap	... two probes per gap
4	10	bottom	0.5% atm	1% atm
5	1	top	of weak shock waves	of such shock waves
5	9-10	top	... shock-wave rise-time..	...shock-wave with a rise time...
5	7	bottom	1 V	0.7 V
6	8	top	delete comma after "seen"	
6	9	top	delete comma after "waves"	
7	10	top	... takes care of ...	... registers ...
10	3	top	$30 < \theta < 180$	$30 < \theta < 150$
10	8	top	Section 7.	Section 8.
10	16 17 18	top	See attached sheet	
12			Replace with attached sheet	

14 To Reference 5, add: "These crystals have been made according to our specifications in size and shape."

15 Table I Delete the last line: 4 190 several 4 2.1 and 4 in the legend.

recorded on a magnetic tape, this time would go down to 10 msec in the present setup.

With two tracks in the chamber, one needs six probes per gap to determine uniquely the spark positions with the present electronics, whose virtue is its extreme simplicity.

The recovery of a probe is also 10 msec (and can probably be reduced with better acoustic impedance matching);this means that within a 0.1-sec Bevatron pulse, ten two-track events per pulse, or 20 tracks per pulse can be accepted, when six probes per gap and the present simple electronics design are used. However, ten tracks per pulse is a sufficient rate for many experiments and this can be accomplished with only two probes per gap. In order to handle more than two events per 10 msec, a different design of the probes (no ringing) and more complicated electronics is needed.

There have been proposed several spark-chamber data-reduction systems -- optical, electrical or electronic -- either as an alternate or as an improvement to the photographic method.[8-12] At this time, it does not seem feasible to discuss the properties of our system in comparison with these proposed systems, since, to our knowledge, operating chambers based on other than photographic or acoustic systems have not been made and tested under running conditions.

Page 10, Line 16, from bottom: The two sentences, beginning with: "Their result on δ..." should be replaced by the following text:

They obtained a one-dimensional resolution of 4 mm at an average distance of about 10 cm (1 part in 25). This implies a rise time of the order of 10 μsec in contrast to 1 μsec (or less) that can be inferred from the early works,[1,2] from numerous shock-wave measurements in plasma discharges, and from our measurements. Since, in order to design a two-dimensional acoustic system which has a resolution that can compete with that of the photographic method, a one-dimensional resolution at least one order of magnitude better than that obtained by Fulbright and Kohler is required, their test has undoubtedly left open the question of the feasibility of the acoustic spark chamber. Nevertheless, it is probably the first conscious attempt to locate sparks by sonic waves. Similar work was subsequently done by Whitehead,[7] who measured the variations of the amplitude of sonic waves with distance by means of a piezoelectric crystal and confirmed the earlier results[2] obtained by a less-advanced technique.

For publication in Nuclear Instruments
and Methods

UCRL-10057

UNIVERSITY OF CALIFORNIA

Lawrence Radiation Laboratory
Berkeley, California

Contract No. W-7405-eng-48

ACOUSTIC SPARK CHAMBER

Bogdan C. Maglić and Frederick A. Kirsten

May 2, 1962

ACOUSTIC SPARK CHAMBER

Bogdan C. Maglić and Frederick A. Kirsten

Lawrence Radiation Laboratory
University of California
Berkeley, California

May 2, 1962

Abstract

Positions of the tracks produced by cosmic rays in a 15-kV four-gap spark chamber were determined by measuring the time of flight T of the shock waves produced by sparks in Argon. A pair of acoustic probes, using barium-titanate piezoelectric transducers is placed in each gap of the spark chamber. Times, T_i in μsec for each probe, i, are measured by a time-sorter and printed 2 sec after the passage of the particle through the chamber; from these, the position and the angle of the track was reconstructed by a program.

With the spark energy of 2 joules, signals of the order of 1 V are obtained from the transducer. These signals are of N-wave form, with the rise-time of 1 μsec or less. The full-width one-dimensional resolution in the spark position is 0.33 mm up to a distance of 52 cm; and 0.41 mm at 1 meter (giving an accuracy to 1:2,500). The full-width spatial resolution, measured with three probes per gap is 0.8 ± 0.4 mm. The time-of-flight *vs* distance dependence is linear up to 2 meters. The recovery time of the probes is 10 μsec, suggesting the possibility of handling up to ten tracks during a long-spill accelerator pulse, with three probes per gap; and up to 20 with six probes per gap.

ACOUSTIC SPARK CHAMBER*

Bogdan C. Maglić and Frederick A. Kirsten

Lawrence Radiation Laboratory
University of California
Berkeley, California

May 2, 1962

1. Introduction

At present, in spark-chamber experiments the position and the angle of particle tracks are obtained by measurements made on stereo photographs of the sparks. We are reporting an alternate method which utilizes sound (shock waves) rather than light produced by sparks. With a pair of microphones (piezoelectric probes) placed between each pair of spark-chamber plates (each gap), the time of flight of the sound signal from the spark to the probes determines uniquely the spark coordinates, x and y, in each gap. From these, one can reconstruct the position and the angle of the track. If this approach is feasible, the process of taking, scanning, and measuring photographs becomes unnecessary. The track coordinates are obtained within seconds after the occurrence of the sparks, in contrast to months of picture analysis. They can be fed to a computer which, in turn, performs the work equivalent to scanning and measuring.

The applicability of this idea critically depends on the resolution with which the shock waves can define the positions of sparks, apart from other factors. We present here the results of our investigations of one-dimensional resolution, spatial resolution, design, operation, possible extensions, and limitations of such an "acoustic" spark chamber.

2. Position of the Spark and the Space Resolution

Consider the ith gap of an n-gap spark chamber. Let the time taken by the sonic wave to travel from the spark to piezoelectric probes 1 and 2 be t_1 and t_2, the velocity of sound in a gas, c, and the distance between the probes, a. The spark coordinates x and y are the point of intersection of two circles of radii $R_1 = t_1/c$ and $R_2 = t_2/c$, whose centers are at (a, 0) and (0, 0):

$$x_i = \frac{R_{2i}^2 - R_{1i}^2}{2a} + \frac{a}{2} \tag{1}$$

$$y_i = \pm (R_{1i}^2 + x_i^2)^{1/2} ,$$

where index i refers to the gap number. We avoid the double-valued y by taking only a half-plane ($y > 0$) i. e. by placing both probes on the same side of the plate ($y = 0$).

The half-width of the resolution in x and y is obtained by differentiating x and y as a function of R_1 and R_2. Since R_1 and R_2 are independent variables, the half-width becomes

$$\sigma_x^2 = \frac{(R_1 dR_1)^2 + (R_2 dR_2)^2}{a^2} , \tag{2}$$

where dR_1 and dR_2 represent the uncertainties in the definition of the spark positions along a straight-line spark probe, i. e. the one-dimension resolution. As it will be seen, dR_1 and dR_2 are nearly independent of R_1 and R_2 (within 1 meter). It is reasonable to assume $dR_1 = dR_2 = \delta$, so that Eq. (2) becomes

$$\sigma_{x_i}^2 = \left(\frac{\delta}{a}\right)^2 \left(R_{2i}^2 + R_{1i}^2\right) . \tag{2'}$$

Similarly, for the uncertainty in y, we have

$$\sigma_{y_i}^2 = \left(\frac{\delta}{y_i}\right)^2 \left[R_2^2 \left(1 - \frac{x_i}{a}\right)^2 + R_{1i}^2 \left(\frac{x_i}{y_i} \left(\frac{\delta}{a}\right)^2\right)\right] . \tag{3}$$

The spatial resolution is the area of an ellipse with axes σ_x and σ_y.

We assume an approximate equality of σ_x and σ_y to the major (whichever σ is larger) and the minor axes of an ellipse; this is true only on the average, since the orientation of the major axis depends on the position $\underline{P}(x, y)$ in the plane of the gap.

From Eqs. (2') and (3) it follows that, in order to obtain the errors at any point $\underline{P}(x, y)$, σ_x, and σ_y, we need only the one-dimensional resolution δ, a constant.

3. Angle of the Track

With only one particle passing through the chamber and for a given z_i, a pair of probes in the ith gap yields a set of values $x_i \pm \sigma_{xi}$ and $y_i \pm \sigma_{yi}$. A least-squares fit to the straight line, defined by equations $x = b + cz$ and $y = d + ez$, determines the coefficients b, c, d, e and their errors $\delta b, \ldots \delta e$. The space angle of the particle passing through the chamber is given by

$$\cos\theta = (c^2 + e^2 + 1)^{-1/2}, \tag{4}$$

and the error by

$$d\theta = \cos^2\theta \cot\theta \, [c(\delta c) + e(\delta e)]. \tag{5}$$

We have tacitly assumed so far that the sound signal always originates at the center of the spark. This is not true for slanted sparks, where the source point is at either top or bottom end of the spark, whichever is nearer to the probe. We note that, when the only quantity of interest is the angle of the track, it is immaterial at which point along the spark the sound originates, as long as this point is the same in every gap. However, if, in addition to the angle, the knowledge of the exact position of the track is required, an appropriate correction program has to be written to shift the y coordinates, upon computation of the angle θ (by an amount proportional to $\sin\theta$).

4. Properties of Shock Waves Produced by Sparks

Much information on properties of the sonic waves produced by sparks is contained in the early works of Töpler[1] and McFarlane[2]. The initial spark consists of a bright core (gas discharge), which is later surrounded by a less bright sheet, the arc, involving only vapor of the electrodes. The amplitude of the pressure wave decreases approximately like 1/R; these pressure-wave pulses are sharp and of a well-defined thickness of the order of a millimeter. Most relevant to our problem is the conclusion, from the work of these authors, that the formation of the pressure wave follows closely in time the formation of the spark. If this conclusion is accepted and compared with the recent study of the spark-formation times by Fischer and Zorn[3] (see Fig. 1), one can see that, e.g. with an 15-kV argon spark chamber, the rise time of the sonic wave of the order of 10^{-7} sec can be easily expected.

At this point it is necessary to outline some of the properties of shock waves in gases. The work of DuMond et al. on ballistic shock-waves is applicable to our situation, and we shall paraphrase some of the points discussed lucidly by these authors.[4] Shock-wave means a propagation of a sudden rise of pressure, density, temperature, and particle velocity. Ordinary sonic waves can be thought of as a special case of shock waves in which changes of all these variables are infinitesimal. The pressure elevation in a weak shock wave is of the order of 0.5% atm (our case), while that of the audible sound is two to three orders of magnitude smaller. The velocity of propagation of shock-waves is amplitude-dependent; the higher-amplitude regions propagate more rapidly than the lower-amplitude regions. Regions of rarifaction (negative pressure) propagate at less than ordinary sonic velocity. As seen in Fig. 2, after a lapse of time the wave takes the form of an "N-wave". Its front propagates faster than ordinary sound, and the excess velocity is given by

$$\frac{D-C}{C} = \frac{\gamma+1}{4\gamma} \frac{p_1-p_0}{p_0}, \tag{6}$$

which with $p_1 = 1.01$ and $\gamma = 1.67$ (argon) becomes 0.2%.

The thickness λ (rise time) of weak shock waves, which determines the time resolution, is proportional to the distance traveled by the wave. This means that in an acoustic spark chamber, the spatial resolution becomes worse for remote sparks.

The spatial resolution of a good spark chamber using the photographic method is $2\sigma = 1$ mm (full width). The one-dimensional resolution is $2\delta = 0.7$ mm. The time resolution required for obtaining such space resolution is equal to $1/C$, where C is the velocity of sound. For argon at room temperature, we have $C = 3.3 \times 10^5$ mm/sec and $\Delta t/\delta = 3$ µsec/mm. Thus, even with a shock-wave rise time $\Delta t = 1$ µsec, i.e., one-tenth as fast as the spark formation time, one can expect $2\delta = 0.33$ mm! (The expected resolution, δ, is 7, 20, and 300% poorer for air, neon, and helium, respectively.)

5. Piezoelectric Probes

The design of the acoustic probe is shown in Fig. 3. The shock waves are transmitted from the gap of the spark chamber to an external piezoelectric transducer through a sonic wave guide. The guide is a solid-pyrex rod, 4 mm in diameter, and 19 cm long. Its receiving end is hemispherically shaped; the other end is flat and is platinum-coated. The transducer is a disc of barium titanate[5] 1 mm thick and 5 mm in diameter, silver-coated on both faces. It is pressed against the flat platinized end of the wave guide. Acoustic contact with it is achieved through an Apiezon grease. The response of the transducer to pressure elevation is about 140 v per bar, and the typical output signal in our experiments was 1 v ($p_1 = 0.005$ bar). We chose to take negative signal from the back end of the transducer, which is held in a lead damper. The whole system -- wave guide, transducer and lead damper -- is acoustically isolated by O-rings and rubber washers. The bellows allows alignment of the probe from outside the chamber.

The shock-wave signals, taken from the transducer without any amplification, are seen in Fig. 4 a and b. The rise time is about 1 µsec, and its length is probably due to the inertia of the transducer rather than the actual shock wave. At farther distances between the spark and the probe, the amplitude decreased. A three-stage amplifier was used; thus the signal appears inverted in Fig. 4 c. Nevertheless, the formation of the N wave can be followed from a, b, c, and particularly d. The noise which appears after the main N-wave signal in Fig. 4d is due to various reflections inside the guide and the lead damper, because our design does not afford adequate acoustic matching. As will be seen, in the next paragraphs, in our measurement of the time of flight of the shock waves, only the leading edge of the signal from the transducers matters; the probe is, for our practical purposes, "deaf" right after the arrival of the leading edge of the signal, and the later ringing is of no importance.

6. Spark Chamber

The chamber, shown in Fig. 5, consists of five 1-in.-thick plates separated by a 1/4-in. gap. These plates are made by stretching 3-mil aluminum foil over aluminum picture frames. A pulse of 15 kV from the presparker was applied to alternate plates whenever a cosmic ray produced a triple coincidence between scintillation counters (one on top of the spark-chamber box, two below). The middle counter was small to allow investigations of different regions of the chamber by "aiming" the cosmic rays in the desired direction. The chamber is filled with 1 atm of argon. There is no clearing field. The capacitance discharged through the chamber was 0.04 μf, so that each spark had an energy of about 2 joules.

~~Nine~~ acoustic probes are mounted through the left side wall of the chamber box. Gaps 1, 2, and 4 (counting from bottom up) have two probes. Gap 3 had three probes in order to measure the experimental errors (see Section 10). The receiving ends of the Pyrex wave guides are 3/4 in. inside the gaps.

On the right side wall, at the height of gap 3, there is a sparker (called the "calibration spark"). It consists of two tungsten wires 1/4 in. apart, and can be pulsed with 15 kV from the thyratron. Its importance is three-fold:

(a) The ratio of the time of flight from the calibration spark to any of the probes in air to the time of flight in argon, gives directly the velocity of the shock-wave in argon in the instantaneous temperature and other physico-chemical conditions. The velocity of sound in air is well-known from the T vs R slope (see Section 9).

(b) The velocity of sound changes with temperatures at a rate of 0.174% per °C. Periodic sparking from the calibration spark takes care of these changes in the course of the experiment, so that the temperature inside the chamber does not have to be controlled.

(c) The probe separation a can be determined by using Eq. (1), since x is known, better than with the finest ruler.

7. Electronics

The principle of our measurement of the time-of-flight of sonic waves can be described as follows. At time $t = 0$ (the occurrence of the spark), a 2-Mc oscillator starts feeding the scaler. After a time lapse $t = T$, the shock wave arrives at the probe, producing a signal at the transducer, which in turn stops the oscillator. Thus, the number of counts on the scaler is equal to the time-of-flight, T, in units of μsec/2.

Actually, T contains also the time of travel through the wave guide, Δt, a known quantity (of the order 30 μsec) which always has to be subtracted from T in order to get the time at which the wave reached the tip of the probe.

Where possible, the electronic system used to measure and record the acoustic time delays in this chamber was assembled using existing pieces of Lawrence Radiation Laboratory standard counting equipment. The equipment included transistorized logic modules, 5-Mc laboratory scalers with electrical read-out, and a scaler print-out. These items were interconnected as shown in the block diagram of Fig. 6.

Basically, the time delays were measured by counting clock pulses during the interval between the spark in the chamber and the arrival of the acoustic wave at the transducer. Ten identical channels capable of recording the information from ten transducers were provided (only nine are actually used).

Refer to Fig. 6. "Start," a signal from the main spark gap, is used as the time reference, and triggers a 28-μsec monostable delay, Delay 1. At the end of the 28-μsec delay period, Delay 1 generates a pulse which sets the flip-flop in each channel -- ten flip-flops in all. The resulting voltage levels from the flip-flops open the ten "and" gates, which thereupon begin passing the clock pulses to the scalers. When a transducer receives an acoustic wave-front, the resulting voltage impulse trips the discriminator, which is biased to reject noise pulses. The output of the discriminator passes through the "Or" gate and resets the corresponding flip-flop. This stops the clock pulses into the scaler of that channel.

At the end of a suitable interval, each scaler contains a number, from which one can determine the acoustic time delay from the spark to the corresponding transducer:

$$T_k = (0.5\, N_k + 28) \pm 0.5\ \mu\text{sec},$$

where T_k is the propagation time of the acoustic wave from the spark to the kth transducer, and N_k is the count stored in the kth scaler.

Delay 1 is provided to prevent premature resetting of the flip-flops because of electrical noise generated by the spark gap and the spark chamber. It accomplishes this by delaying the setting of the flip-flops until this electrical noise has disappeared.

Sometimes a transducer may not produce a signal of sufficient voltage to trip the discriminator. For this reason, a second monostable delay,

Delay 2, is provided, which delivers a second reset pulse to all ten flip-flops 2 msec after the start pulse. The only action of this second reset pulse is to reset any flip-flops that have not previously been reset by their transducer. Since 2 msec is longer than the longest possible acoustic delay in our chamber, it is readily apparent which scalers contain invalid counts.

Delay 2 also delivers a print command to the scaler print-out. The print-out then produces a printed record, on paper tape, of the count stored in each scaler. The printing process consumes about 2 sec, after which the scalers are reset, and the system is ready to record another spark-chamber event.

The present system, with its read-out time of 2 sec, is not suited for recording spark-chamber events at the rate at which the chambers themselves can operate. A system using a magnetic-core buffer store has been proposed. It would record the data from a spark chamber having 100 transducers onto a magnetic tape in less than 0.3 sec.

8. Angular Response of Piezoelectric Probes

A knowledge of the response of our sonic probes to the sound signal as a function of the angle of incidence is essential to our method. We have used a movable spark gap in air, consisting of two 10-mil tungsten wires 0.25 in. apart, for these measurements. Sparks are produced by 15-kV thyratron pulses, and the measurements have been done on a large table covered with the graph paper.

As seen in Fig. 7, the amplitude of the signal from the transducer has its peak at $\theta=90$ deg and decreases to about one-half of its maximum value at 0 and 180 deg. This variation is qualitatively consistent with the change of the effective area of the hemispheral tip of the probe upon which the plane wave impinges in this angular interval, and its effects can be easily removed by an appropriate amplification.

The upper portion of Fig. 5 shows that, within our experimental errors, the time-of-flight measurements of the shock wave is independent of the angle of incidence θ, at least in the angular range 30 deg $< \theta <$ 180 deg. Since we have not used a turntable in these angular distribution measurements, our knowledge of the distance at various angles is not better than 0.5 mm.

9. One-dimensional Resolution

We have measured the one-dimensional resolution, 2δ, in air with the movable spark gap, described in Section 7. At each distance R, the distribution of the time of flight of the sonic signal, T, has been plotted in units of 1/2 μsec. The results are shown in Fig. 8a and in Table I. The resolution decreases as the distance increases, but even at 1.021 meter it is $2\delta = 0.4$ mm, giving an accuracy of 1 part in 2,550. As seen in Fig. 9, the resolution is even better when the sound passes between the plates of the spark chamber. In the course of this work we have learned of the attempts made by Fulbright and Kohler[6] to locate the spark position in a self-quenching counter (one-dimensional device) by means of a piezoelectric transducer. Their result on δ is also listed in Table I. Similar results have been obtained by Whitehead.[7]

As a check of the reliability of our measuring system, we have plotted the time T vs distance R, which is expected to be a straight line. Figures 10a and 10b show the experimental points for various probes and distances up to 2 meters. The errors are equal or smaller than the size of the points. The slope of the straight line determines the sound velocity, C. Note that the line does not extrapolate to T = 0 at R = 0. This has to do with the delay of about 28 μsec (Section 7) in the "start" of our clock (2-Mc oscillator), inserted to account for the passage of the sonic waves through the guide. This delay is never exactly equal to the actual passage time Δt. The difference of these two times, δt, has to be measured for each probe; it is a constant of the probe and is subtracted from the observed time T in the computer program.

10. Spatial Resolution σ_x, σ_y

According to Eqs. (2') and (3), the spatial resolution σ is determined once the one-dimensional resolution δ is known. However, imperfections in the system are bound to exist, and a direct measurement of σ_x and σ_y is required in order to check the values obtained with the formulae. This is done by using three probes per gap. If the probes are numbered 1, 2, and 3, each pair will determine the spark points: $P_{12}(x_{12}, y_{12})$; $P_{13}(x_{13}, y_{13})$; and $P_{23}(x_{23}, y_{23})$. Then, the average experimental spatial resolution, σ^{exp}, can be determined from:

$$2\sigma_x^{exp} = \frac{1}{2}\left(|x_{12}-x_{13}| + |x_{12}-x_{23}|\right) \tag{7}$$

$$2\sigma_y^{exp} = \frac{1}{2}\left(|y_{12}-y_{13}| + |y_{12}-y_{23}|\right). \tag{8}$$

With three probes on the measuring table and with the movable spark gap, the values of σ_x and σ_y that we obtained are shown in Table II. The results obtained inside the spark chamber under operating conditions are shown in Fig. 11. The upper portion shows an example of 16 sparks on 1-cm^2 area. The triangles are drawn through three points P_{12}, P_{13}, and P_{23}. Most of them lie within an area smaller than 1 mm^2. The lower portion shows the distribution of σ^{exp}, according to Eqs. 7 and 8, for 75 sparks. The average is $\sigma = 0.4$, giving:

$$2\sigma^{exp} = 0.8 \pm 0.2 \text{ mm}.$$

11. Extensions and Limitations of the Acoustic Spark Chamber

With the above described system, which uses nine probes, the spark coordinates are printed 2 sec after passage of the particle through the chamber. If the printer were replaced by a system in which the data are recorded on a magnetic tape, this time would go down to 10 msec in the present setup.

With two tracks in the chamber, one needs six probes per gap to determine uniquely the spark positions with the present electronics, whose virtue is its extreme simplicity.

The recovery of a probe is also 10 msec (and can probably be reduced with better acoustic impedance matching); this means that within a 0.1-sec Bevatron pulse, ten two-track events per pulse, or 20 tracks per pulse can be accepted, when six probes per gap and the present simple electronics design are used. This is sufficient for many experiments. However, in order to handle more than two events per 10 msec, a different design of the probes (no ringing) and more complicated electronics is needed.

There have been proposed several spark-chamber data-reduction systems -- optical, electrical or electronic -- either as an alternate or as an improvement to the photographic method.[8, 9, 10, 11, 12] It does not seem feasible to us, at this time, to discuss the properties of our system in comparison with these proposed systems.

Acknowledgment

Thanks are due to Drs. William A. Wenzel, Denis Keefe, Leroy T. Kerth, and John Thresher; Messers Ching Lin Wang, and Gerald L. Schnurmacher; and other members of the Lofgren Group for instrumentation and advice; to Dr. Edward J. Lofgren for his continuous interest; to Dr. Robert Ely for his help in some tests; to Mr. Donald H. F. Zurlinden for programming; to Messers Dick A. Mack and William R. Baker for help in early stages of this work; and to Messers Louis A. Biagi, C. Wayne McMullen, and particularly Leonard B. Proehl for invaluable assistance throughout this work.

References

*This work was done under the auspices of the U. S. Atomic Energy Commission.

†Present address: CERN, Geneva, Switzerland.

1. M. Töpler, Ann. Physik 17, 1043 (1908).
2. W. McFarlane, Phil. Mag. 17, 24 (1934).
3. J. Fischer and G. T. Zorn, Rev. Sci. Instr. 32, 499 (1961).
4. J. W. DuMond, E. R. Cohen, W. K. Panofsky, and E. Deeds, J. Acoust. Soc. Am. 18, 97 (1946).
5. Ceramic "B", Clevite Electronics Components, Cleveland, Ohio.
6. H. W. Fulbright and D. Kohler, University of Rochester Report NYO-9540, 1961, unpublished.
7. C. Whitehead, AERE, Harwell, private communication.
8. H. Gellerntner, Nuovo cimento 22, 631 (1961).
9. Jerome A. G. Russell, A Proposal for Developing an Automatic Processing System for Spark-Chamber Experiments, Lawrence Radiation Laboratory Report UCID-1374, June 8, 1961.
10. G. Culligan, D. Harting, and N. H. Lipman, CERN preprint 61-25 (1961).
11. G. Charpak, CERN preprint 1962 (unpublished).
12. F. Krienen, CERN preprint, 1962 (submitted to this journal).

Table I. One-dimensional resolution 2δ at various distances R, measured in air. Measurements 1 through 4 refer to: (1) movable spark gap on the measuring table; (2) calibration spark in spark chamber at θ = 90 deg incidence; (3) the same at θ = 35 deg; (4) reference 6.

Measurement	Distance R (mm)	Resolution Δt(μsec)	Resolution 2δ(mm)	Percent resolution
1	121	0.9	0.33	0.273
	221	0.9	0.33	0.150
	321	0.9	0.33	0.105
	421	0.9	0.33	0.078
	521	0.9	0.33	0.065
	621	1.15	0.41	0.066
	1021	1.15	0.41	0.04
	2021	1.70	0.60	0.03
2	287	0.6	0.21	0.073
3	287	0.9	0.33	0.119
4	190	several	4	2.1

Table II. Average experimental spatial resolution obtained with three probes. Resolutions σ_x and σ_y are not given separately.

Measurement	Average distance from center probe R(mm)	Average resolution 2σ (mm)
1[a]	200	0.59 ± 0.2
2[b]	200	0.8 ± 0.4

[a]Measurements on the table, with movable gap, in air.

[b]Measurements in the argon-filled spark chamber with cosmic rays.

Figure Legends

Fig. 1. Experimental values of the spark formation time in argon and in argon and alcohol as a function of the applied voltage for gap lengths 0.062, 0.26, and 0.52 in. (from Fischer and Zorn, reference 3).

Fig. 2. Formation of N-waves. The ordinates are $(P_1 - P_0)$, where P_0 is the atmospheric pressure (from DuMond et al., reference 4).

Fig. 3. Design of the acoustic probe and its spatial relation to the spark chamber. (1) Pyrex wave-guide; (2) O-rings; (3) ring made of paper tape for setting the wave-guide position; (4) platinum coating; (5) barium-titanate transducer; (6) electrodes for the voltage signal from the transducers; (7) lead damper; (8) rubber damper; (9) aluminum screw; (10) lucite jacket; (11) stainless steel bellows; (12) wall of the spark-chamber box; (13) spark-chamber plates.

Fig. 4. Photographs of the oscilloscope traces of signals taken from transducers of the acoustic probe: (a) direct signal without amplification at $R \cong 2$ cm; (b) the same at $R \cong 4$ cm; (c) shape of the amplified and inverted signals at $R \approx 28$ cm (expanded); (d) the appearance of the shock-wave signal as it arrived from a distance of about 30 cm. The "ringing" of the probe behind the first N-wave lasts 10 msec; (e) the signal seen in (d), after the discriminator—pulse-shaper circuit. This is the "stop" signal, which turns off the oscillator, as seen in (f); (g) and (h) are examples of signals from two probes placed in one gap of the spark chamber. Probe 2 in (h) shows an example of electromagnetic pickup at about 100 μsec which sometimes can trigger the "stop" signal and confuse the measurement.

Fig. 5. (a) Photograph of the spark chamber. The acoustic probes are seen at the left (see section 6); (b) and (c) show examples of the sparks due to cosmic rays.

Fig. 6. Block diagram of electronics (see section 7).

Fig. 7. Angular response of acoustic probes. The lower part of the figure shows the angular distribution of the voltage amplitude of the pulses taken from the transducer, while the upper part shows the angular distribution of the time of flight.

Fig. 8. (a) One-dimensional resolution at various distances R. Here N is the number of sparks.

Fig. 9. One-dimensional resolution inside the chamber, measured with the calibration spark, at constant R but two different angles of incidence. Upper portion, $\theta = 90$ deg; lower, $\theta = 35$ deg. Here N is the number of sparks.

Fig. 10. (a) Time of flight T vs distance R for two probes.

(b) Time of flight vs distance R obtained from the data in Fig. 8(a).

Fig. 11. Experimental spatial resolution inside spark-chamber gap No. 3, obtained with three probes. The upper portion shows an example of 16 sparks on a 1-cm^2 area. The corners of the triangles are the spark position as "seen" by different pairs of probes (pairs 1-2, 1-3, and 2-3); the lower portion shows the distribution of σ^{exp} according to Eqs. (7) and (8) for 75 sparks.

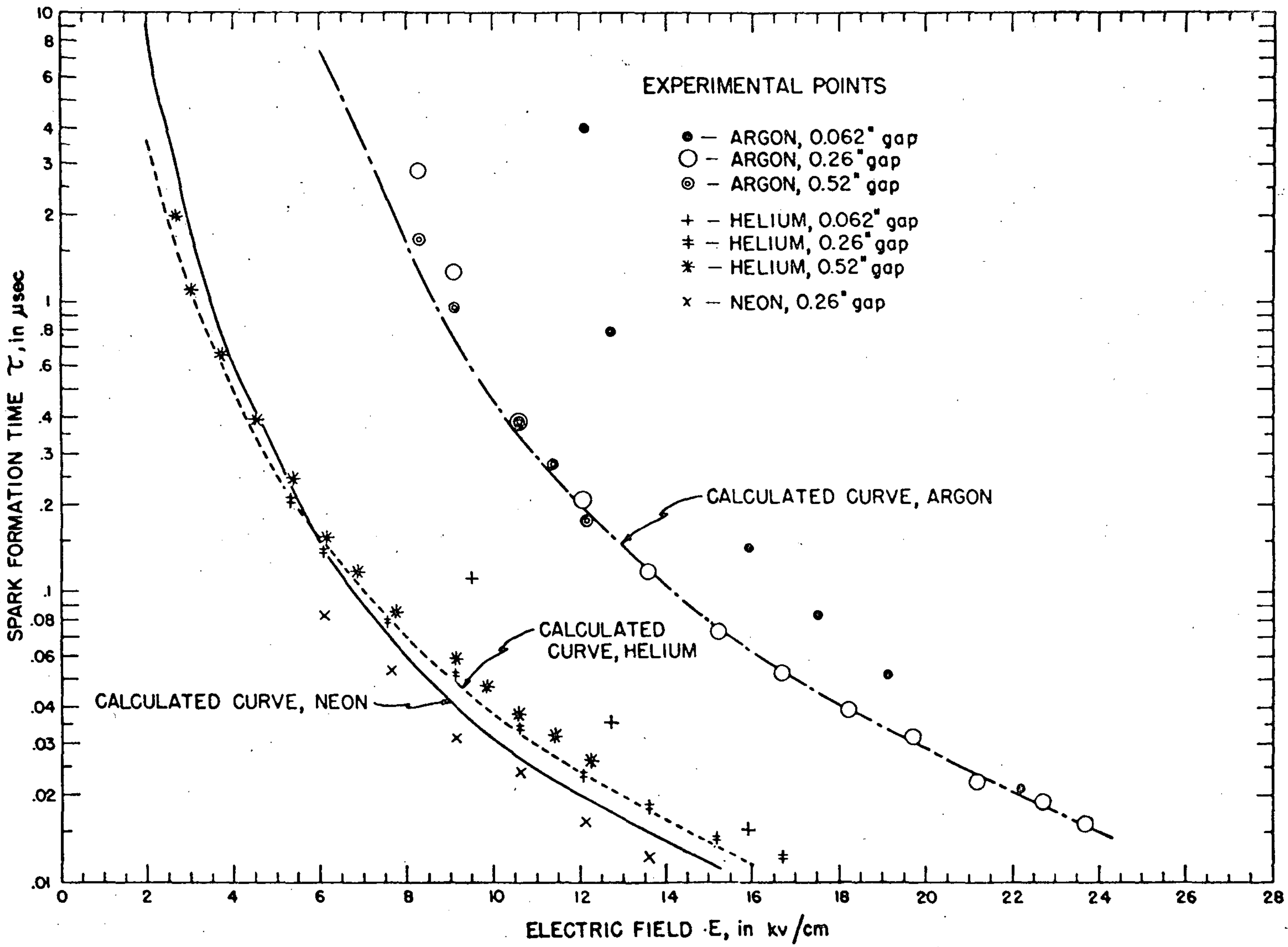
EXPERIMENTAL POINTS
— ARGON, 0.062" gap
— ARGON, 0.26" gap
— ARGON, 0.52" gap
— HELIUM, 0.062" gap
— HELIUM, 0.26" gap
— HELIUM, 0.52" gap
— NEON, 0.26" gap
CALCULATED CURVE, ARGON
CALCULATED CURVE, HELIUM
CALCULATED CURVE, NEON
SPARK FORMATION TIME τ, in μsec
ELECTRIC FIELD E, in kv/cm

Fig. 1

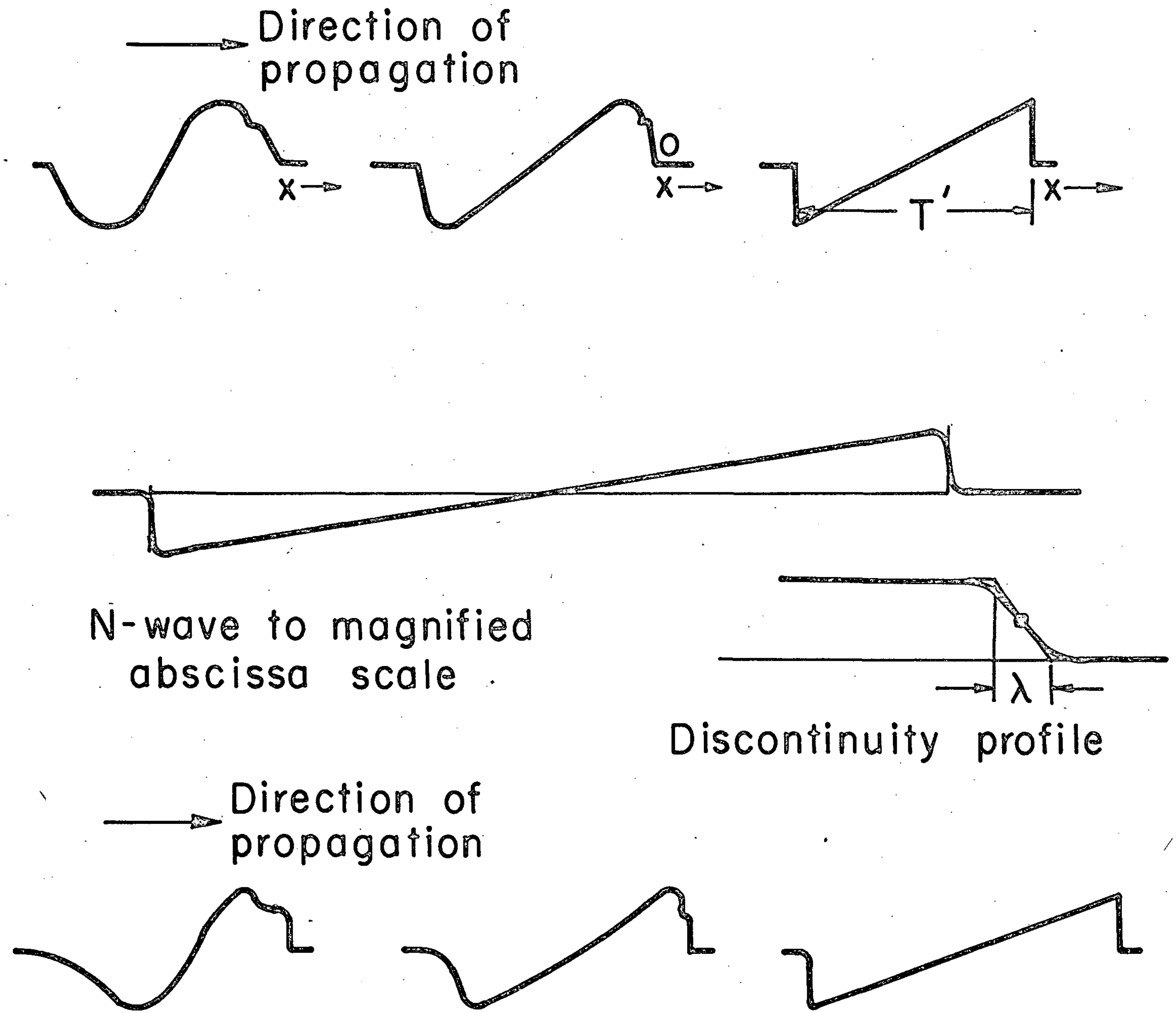
Direction of propagation
x
o
x
T′
x
N-wave to magnified abscissa scale
λ
Discontinuity profile
Direction of propagation

Fig. 2

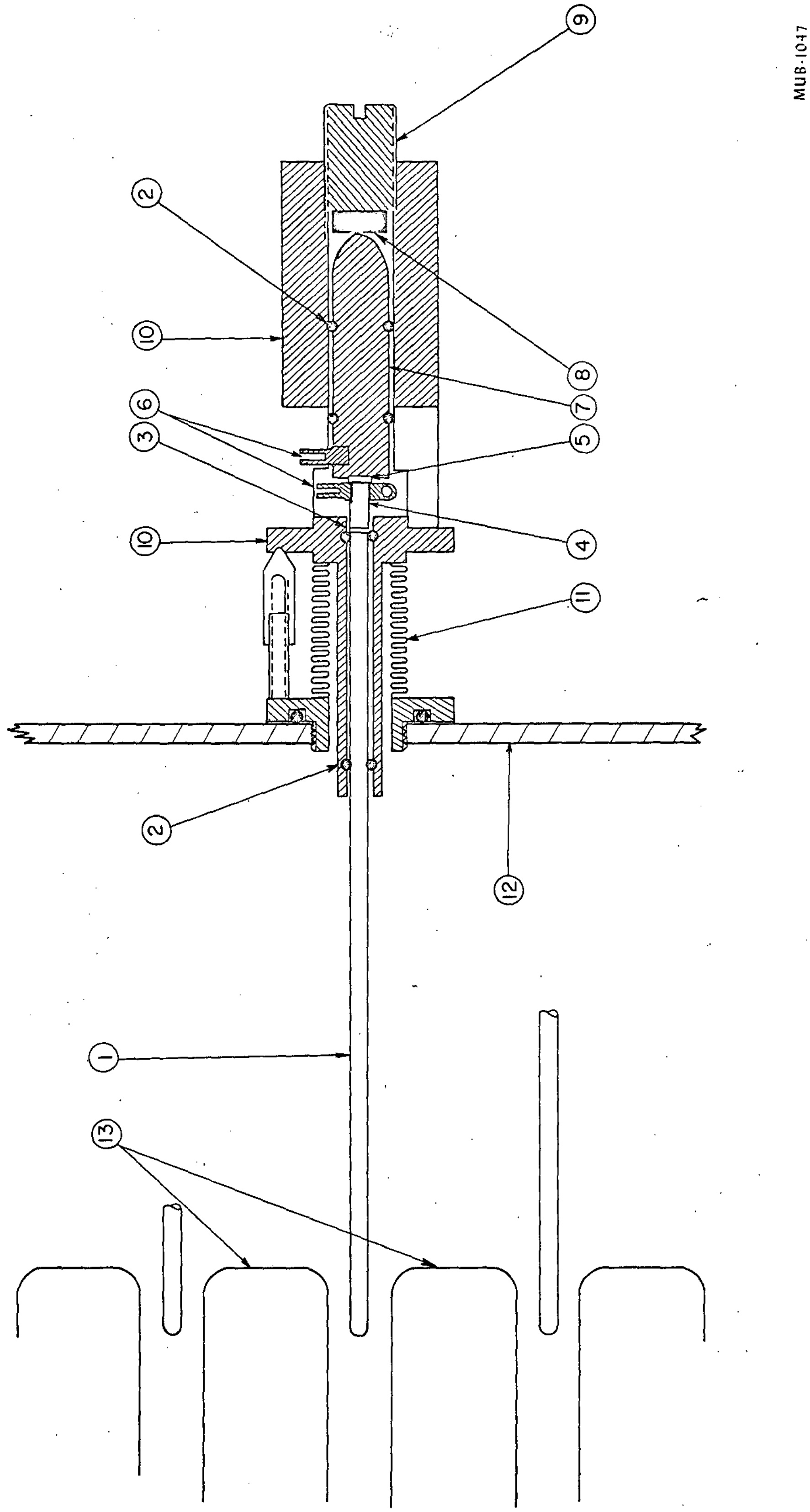

Fig. 3

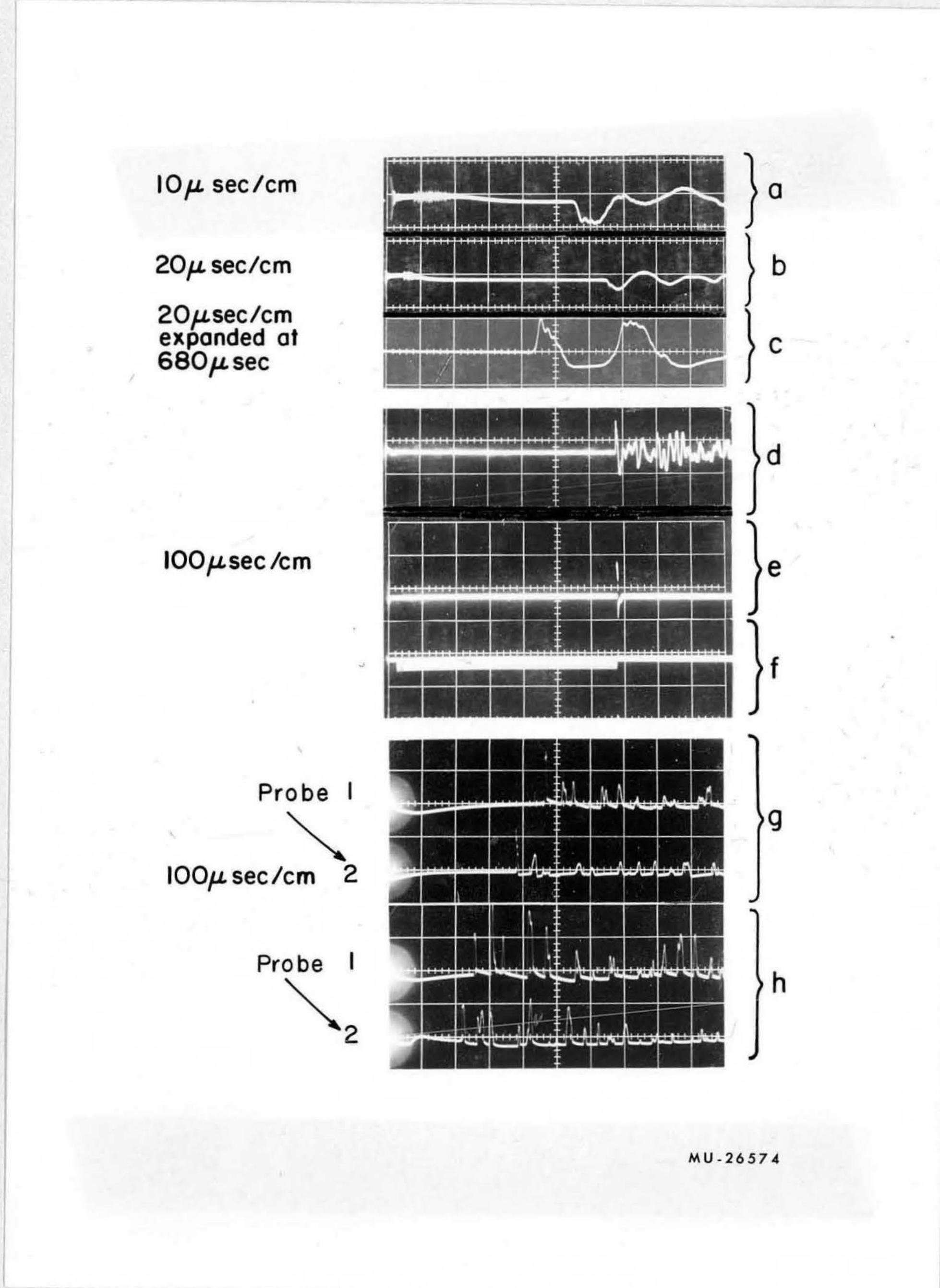
10μ sec/cm
a
20μ sec/cm
b
20μsec/cm expanded at 680μsec
c
d
100μsec/cm
e
f
Probe 1
2
100μ sec/cm
g
Probe 1
2
h
MU-26574

Fig. 4

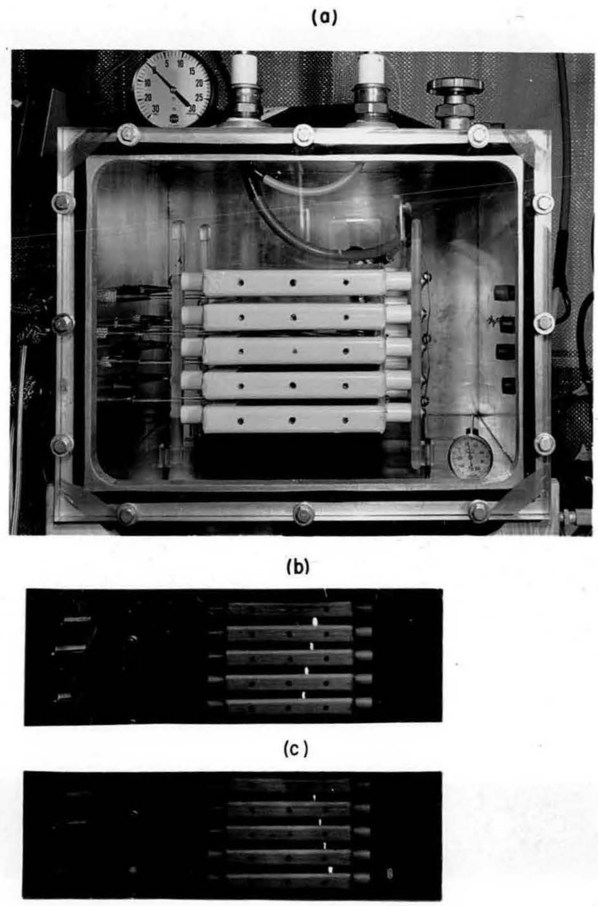

Fig. 5

Fig. 6

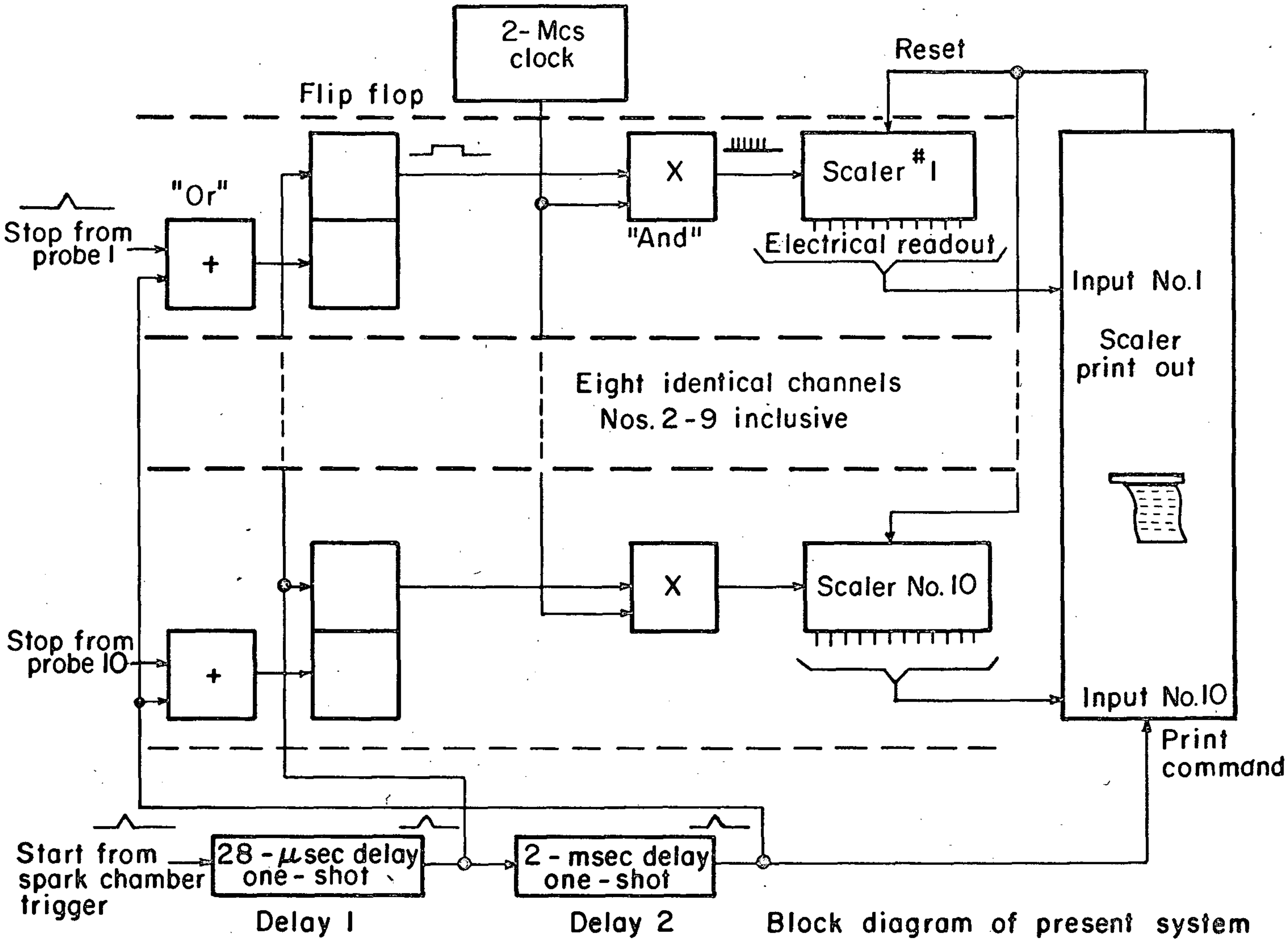

Block diagram of present system

MU-26573

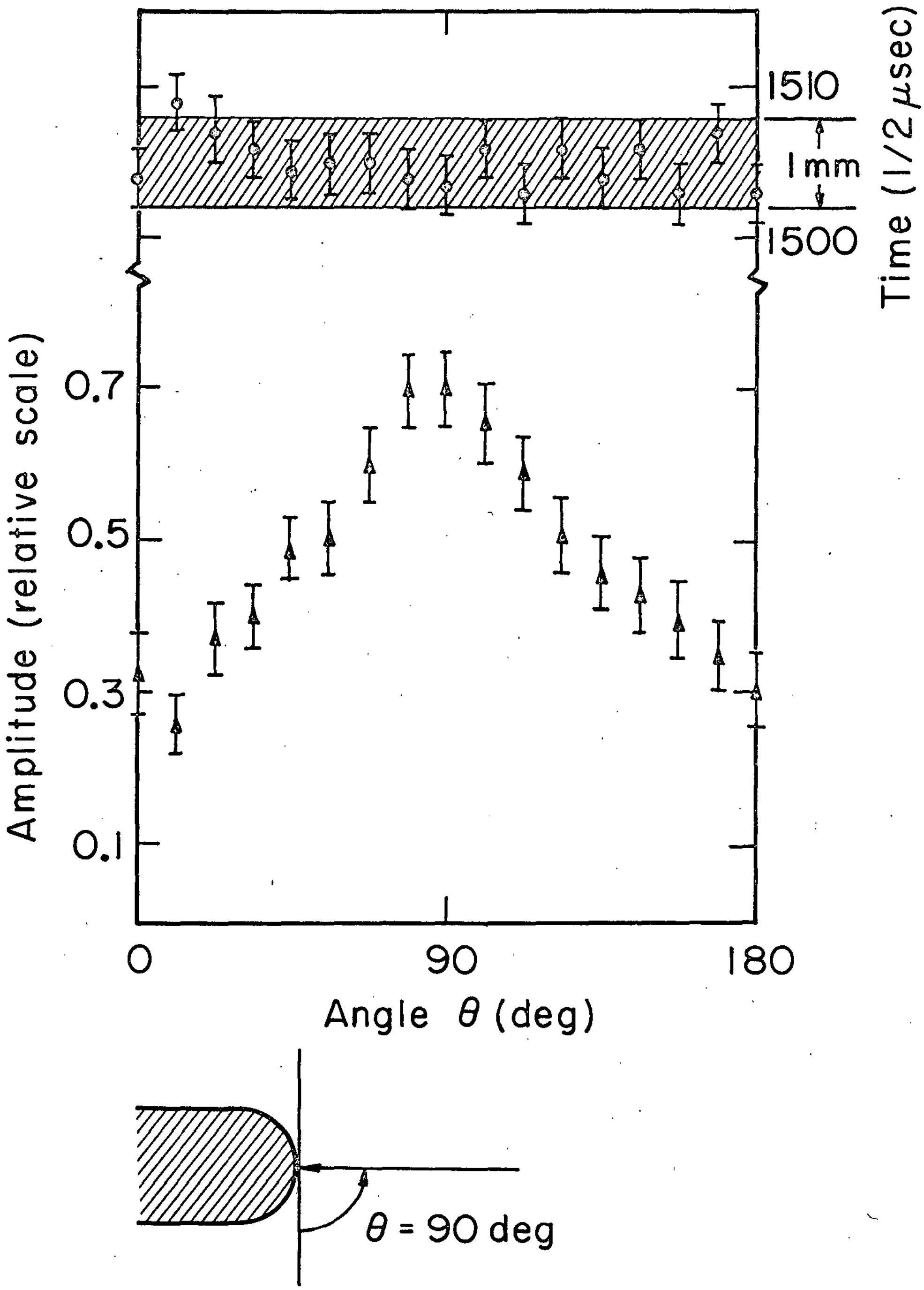

MU-26325

Fig. 7

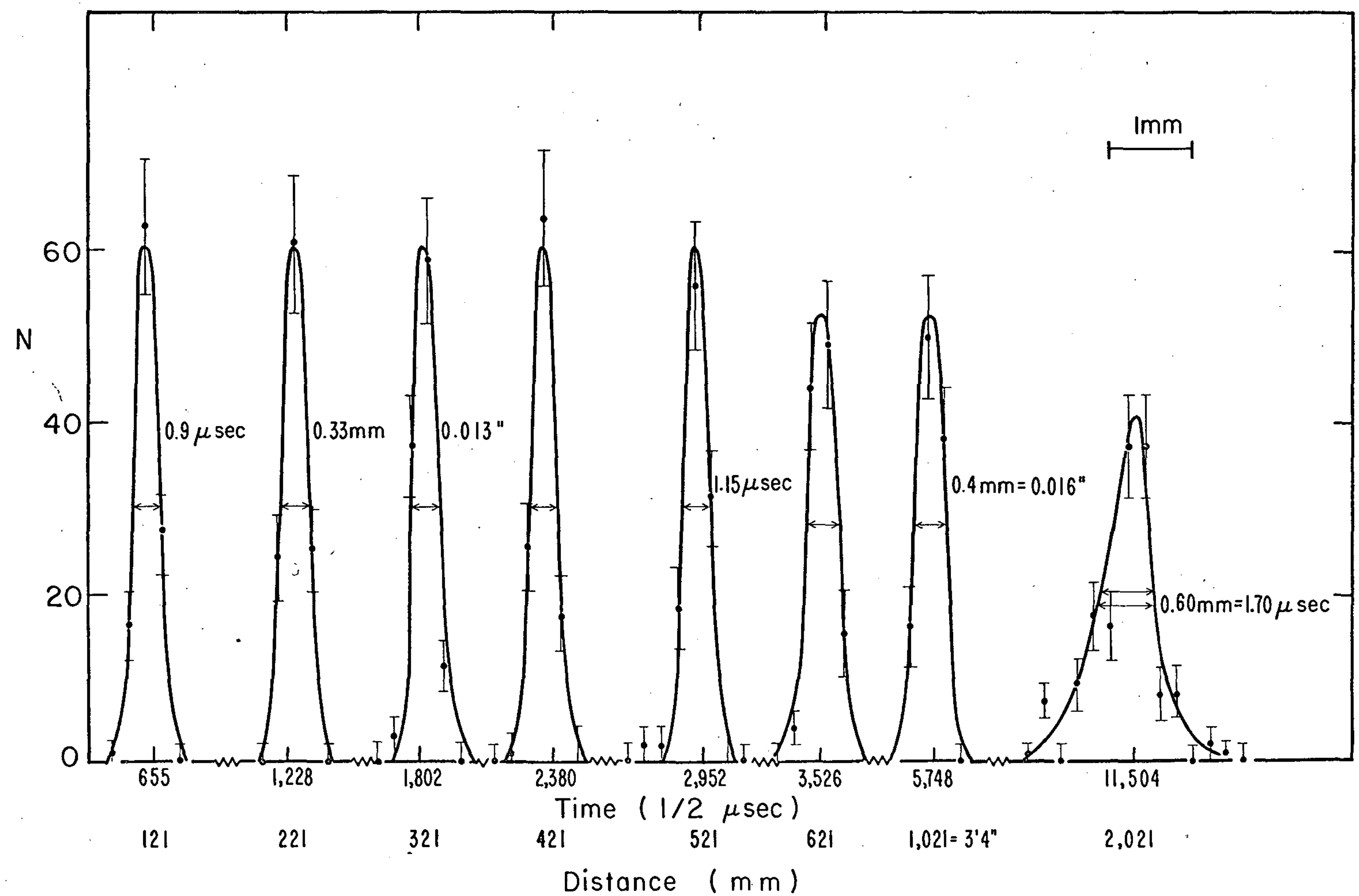

Imm
60
40
20
0
N
0.9 μ sec
0.33mm
0.013"
1.15 μsec
0.4 mm = 0.016"
0.60mm = 1.70 μ sec
655
1,228
1,802
2,380
2,952
3,526
5,748
11,504
Time (1/2 μsec)
121
221
321
421
521
621
1,021 = 3'4"
2,021
Distance (mm)

Fig. 8

MUB-996

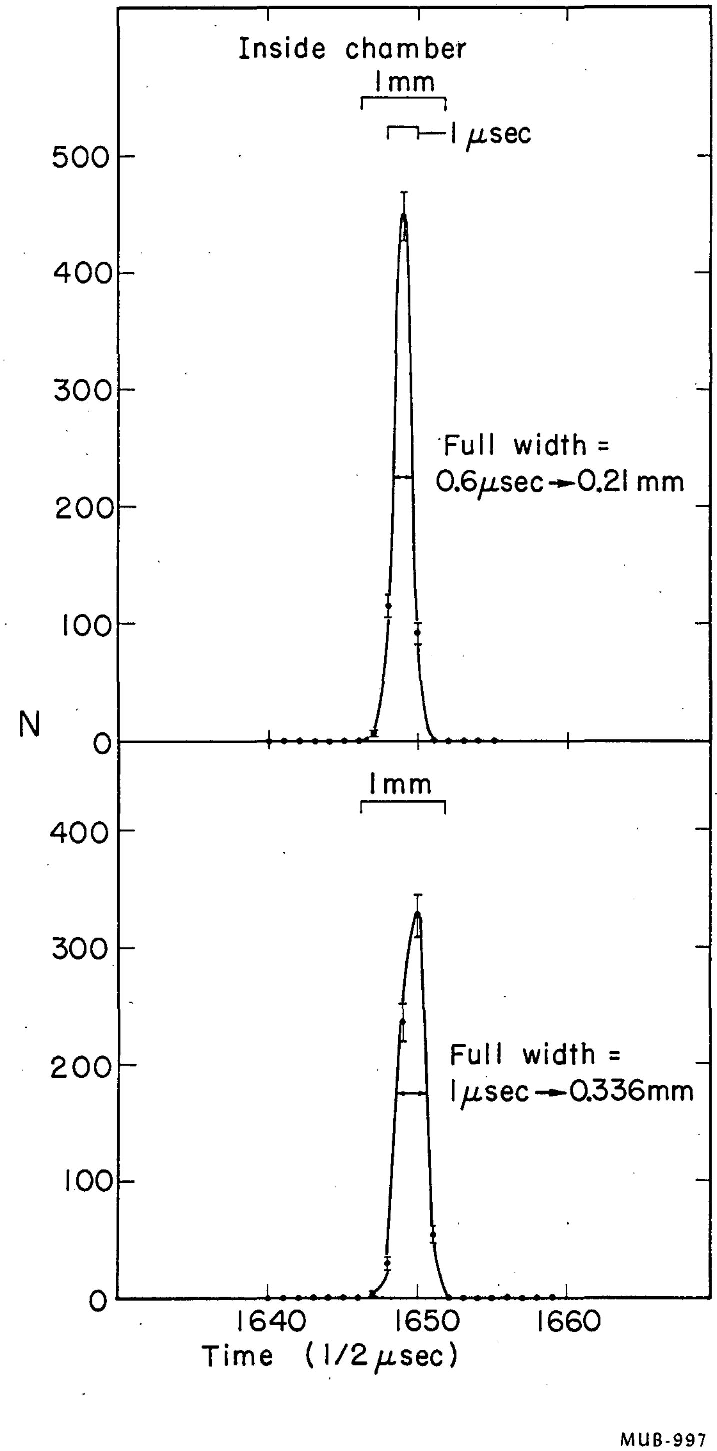
Inside chamber
1mm
1 μsec
Full width =
0.6μsec → 0.21 mm
N
1mm
Full width =
1μsec → 0.336mm
Time (1/2 μsec)
MUB-997

Fig. 9

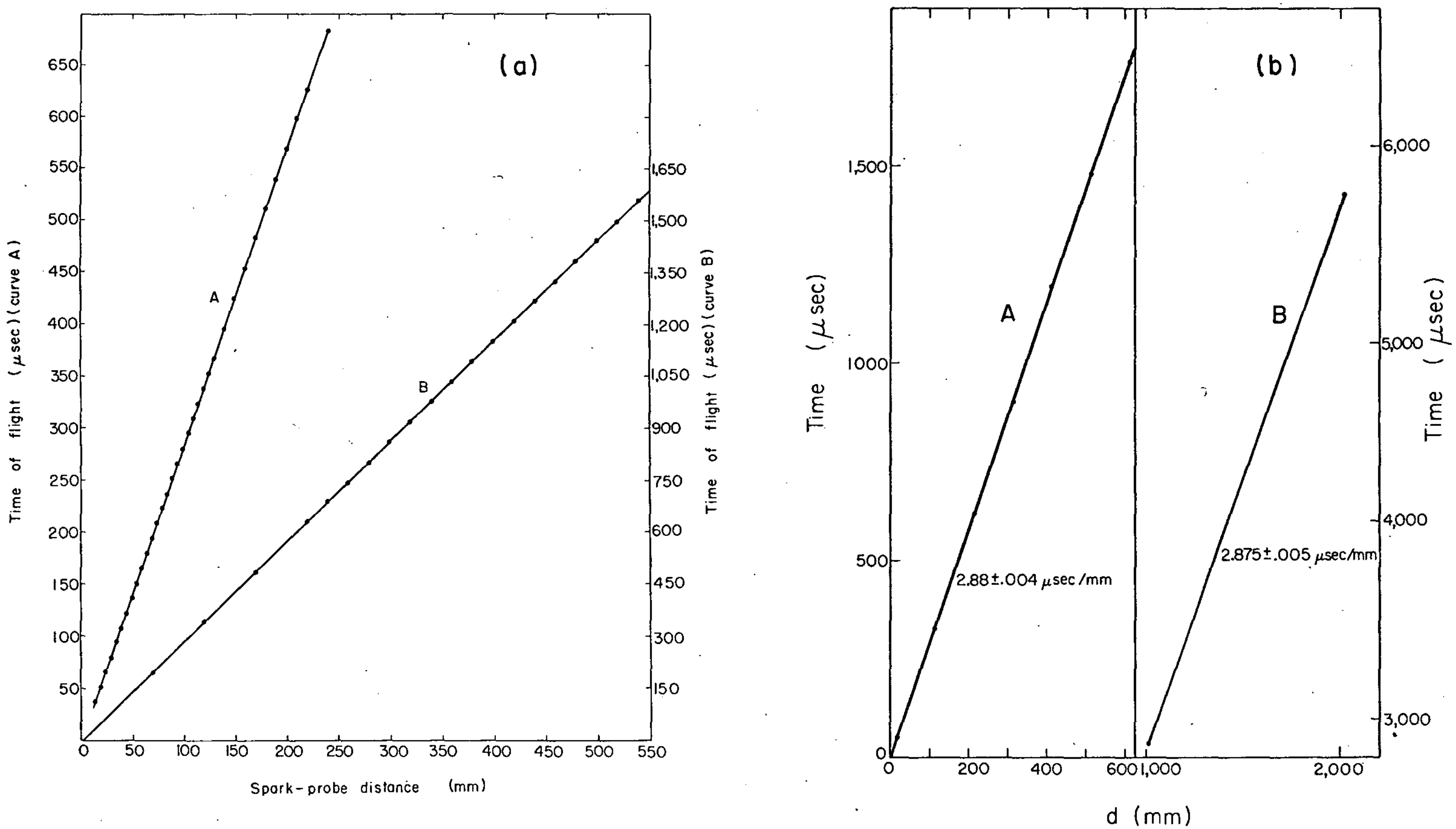

Fig. 10

MUB-1041

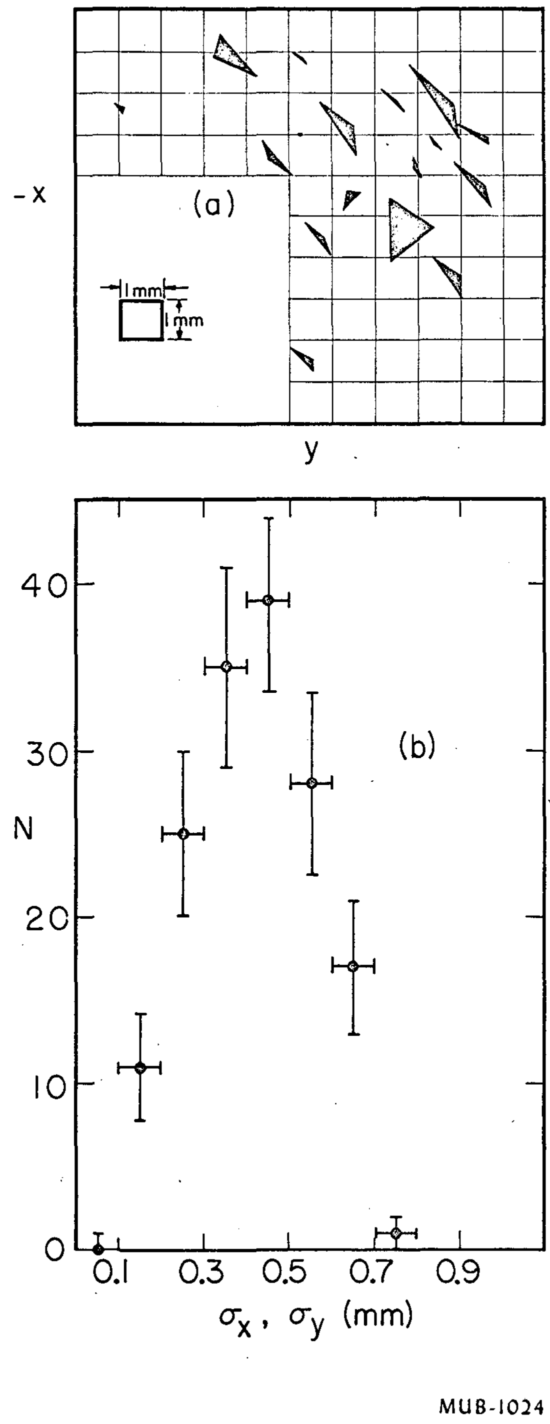
-x
(a)
1mm
1mm
y
40
30
20
10
0
N
(b)
0.1
0.3
0.5
0.7
0.9
σ_x, σ_y (mm)
MUB-1024

Fig. 11